Osteosarcoma stem cells resist chemotherapy by maintaining mitochondrial dynamic stability via DRP1

BOREN TIAN, YAXUAN WU, XIAOYUN DU and YAN ZHANG

MOE Key Laboratory of Gene Function and Regulation, School of Life Sciences, Sun Yat-sen University, Guangzhou, Guangdong 510275, P.R. China

Received July 23, 2024; Accepted September 27, 2024

DOI: 10.3892/ijmm.2024.5451

Abstract. Osteosarcoma malignancy exhibits significant heterogeneity, comprising both osteosarcoma stem cells (OSCs) and non-OSCs. OSCs demonstrate increased resistance to chemotherapy due to their distinctive cellular and molecular characteristics. Alterations in mitochondrial morphology and homeostasis may enhance chemoresistance by modulating metabolic and regulatory processes. However, the relationship between mitochondrial homeostasis and chemoresistance in OSCs remains to be elucidated. The present study employed high-resolution microscopy to perform multi-layered image reconstructions for a quantitative analysis of mitochondrial morphology. The results indicated that OSCs exhibited larger mitochondria in comparison with non-OSCs. Furthermore, treatment of OSCs with cisplatin (CIS) or doxorubicin (DOX) resulted in preserved mitochondrial morphological stability, which was not observed in non-OSCs. This finding suggested a potential association between mitochondrial homeostasis and chemoresistance. Further analysis indicated that dynamin-related protein 1 (DRP1) might play a pivotal role in maintaining the stability of mitochondrial homeostasis in OSCs. Depletion of DRP1 resulted in the disruption of mitochondrial stability when OSCs were treated with CIS or DOX. Additionally, knocking out DRP1 in OSCs led to a reduction in chemoresistance. These findings unveil a novel mechanism underlying chemoresistance in osteosarcoma and suggest that targeting DRP1 could be a promising therapeutic strategy to overcome chemoresistance in OSCs. This provided valuable insights for enhancing treatment outcomes among patients with osteosarcoma.

Correspondence to: Professor Yan Zhang, MOE Key Laboratory of Gene Function and Regulation, School of Life Sciences, Sun Yat-sen University, 135 Xingang Xi Road, Guangzhou, Guangdong 510275, P.R. China
E-mail: zhang39@mail.sysu.edu.cn

Key words: osteosarcoma, cancer stem cells, chemoresistance, mitochondrial dynamics

Introduction

Mitochondria are known as the powerhouses of the cell and influence key signaling pathways related to cellular homeostasis, proliferation and apoptosis (1-3). The study of mitochondrial dynamics and biogenesis has attracted significant attention in recent years due to its vital role in elucidating diverse biological phenomena, including the process of apoptosis in cancer cells (4-7). Mitochondrial homeostasis is regulated by two opposing processes: Fusion and fission (8). Mitochondria can fuse to form larger networks or undergo fission into smaller mitochondria (1). These distinct alterations in mitochondrial morphology can trigger different metabolic and regulatory processes, thereby enhancing the chemoresistance of cancer cells (5,6,9).

Evidence suggests a close association between dysregulated mitochondrial homeostasis and tumorigenesis, offering a novel perspective for comprehending intricate oncogenic processes. Mitochondrial fission has been observed in neoplastic cells across various solid tumors. Research has demonstrated that dysregulated mitochondrial homeostasis, characterized by increased fission or weakened fusion, is commonly found in numerous types of cancer, resulting in mitochondrial fragmentation (10-13). The process of mitochondrial fusion, which involves the merging of mitochondrial membranes, is facilitated by mitofusin1 (MFN1), mitofusin2 (MFN2) and optic atrophy 1 (OPA1). By contrast, mitochondrial fission is regulated by DRP1, which forms a ring-like structure on the outer mitochondrial membrane to facilitate the constriction and division of mitochondria. Notably, in most types of cancer, the expression of the key mitochondrial fission gene DRP1 is upregulated, while the expression of the mitochondrial fusion gene MFN2 is downregulated (14-17). These finding suggest a potential role for mitochondrial homeostasis in tumor progression.

Dysregulated mitochondrial homeostasis may play a pivotal role in cancer chemoresistance. The mechanisms underlying chemoresistance in tumors are complex, involving multiple cellular processes and molecular pathways. One hypothesis suggests that mitochondrial homeostasis contributes to the acquisition of anti-apoptotic capabilities. The release of cytochrome *c* from the mitochondrial outer membrane, triggered by changes in membrane permeability, initiates a cascade leading to programmed cell death (18). Changes in

mitochondrial homeostasis directly affect the permeability of the mitochondrial outer membrane, potentially inhibiting the shifts in membrane potential induced by chemotherapeutic agents and thereby granting cells anti-apoptotic properties (4).

In addition to mitochondrial homeostasis, cancer heterogeneity plays a crucial role in chemoresistance. In osteosarcoma, a highly heterogeneous malignant tumor that predominantly affects adolescents (19), its heterogeneity driven by the plasticity of osteosarcoma cells, contributes to the high chemoresistance observed in this disease. Osteosarcoma cells can be categorized into two subpopulations: osteosarcoma stem cells (OSCs) and non-osteosarcoma stem cells (non-OSCs). 'OSCs' refer to osteosarcoma cells that exhibit stem cell properties, such as self-renewal, differentiation capacity, chemoresistance and high tumorigenic potential (20). By contrast, 'non-OSCs' refers to osteosarcoma cells that do not possess these stem cell properties (20). The high chemoresistance exhibited by OSCs presents a significant challenge for eradication, complicating the clinical management behind osteosarcoma (21,22). However, the underlying mechanism of the difference in chemoresistance between OSCs and non-OSCs are still unknown remain to be elucidated.

Given the potential role of mitochondrial homeostasis in cancer chemoresistance, the present study aimed to investigate the disparities in mitochondrial dynamic changes between OSCs and non-OSCs and study the involvement of these alterations in mechanisms underlying chemoresistance. Exploring mitochondrial dynamics in osteosarcoma could elucidate chemoresistance mechanisms and enhance therapeutic strategies, potentially improving patient outcomes.

Materials and methods

Cell culture. The human osteosarcoma cell line MG-63 was obtained from the Cell Bank of the Chinese Academy of Sciences (cat. no. TCHu124) and maintained as monolayer cultures in Dulbecco's modified Eagle's medium/F12 (DF12; cat. no. D8900; MilliporeSigma) supplemented with 5% fetal bovine serum (FBS; MilliporeSigma), penicillin (100 U/ml) and streptomycin (100 U/ml) in an incubator at 37˚C with 5% CO_2. The human embryonic kidney cells 293T were obtained from the Cell Bank of the Chinese Academy of Sciences (cat. no. SCSP-502) and maintained as monolayer cultures in Dulbecco's modified Eagle's medium-high glucose (cat. no. D5648; MilliporeSigma) supplemented with 5% fetal bovine serum (FBS; MilliporeSigma), penicillin (100 U/ml) and streptomycin (100 U/ml) in an incubator at 37˚C with 5% CO_2. For OSCs, the MG-63 was cultured in serum-free DF12 supplemented with 5 factors (5F), including 10 μg/ml human insulin, 5 μg/ml human transferrin, 10 μM 2-aminoethanol, 10 nM sodium selenite, 10 μM mercaptoethanol, 5 mg/ml bovine serum albumin and 5 ng/ml transforming growth factor-β, as previously described (23,24).

Vectors and cell transfection. The knockout of *DRP1* by CRISPR/Cas9 in the MG-63 cells was performed using the 2nd Lenti-Crispr-vector system (cat. no. 49535; Addgene, Inc.). Lentivirus (5 μg) was amplified from 293T packaging cells with pSPAX2 and pMD2G (cat. nos. 12260 and 12259; Addgene, Inc.) helper plasmids (quantity of plasmids ratio was pSPAX2:pMD2G:Lentivirus=3.75:1.25:5). The virus-containing supernatants were collected at 48 h following transfection. The supernatants, with 5% PEG8000 were centrifuged at 4,000 x g for 2 h at 4˚C to concentrate the lentiviral particles, diluted in 200 μl PBS and then stored at -80˚C. The MG-63 cells were then transfected with the lentivirus (40 μl lentivirus in 2 ml DF12; with a multiplicity of infection of 10 for lentiviral vectors) for 8 h at 37˚C then selected with 1 μg/ml puromycin (cat. no. A1113803; Gibco; Thermo Fisher Scientific, Inc.). The time interval between transduction and subsequent experimentation was 48 h to allow sufficient expression of the transgene. The single guide (sg)RNA-DRP1 primers were as follows: Sequence 1, AUAUUCUGUUUUCAGAGCAG and sequence 2, GAGCUCAGUGCUAGAAAGCC.

RNA isolation and reverse transcription-quantitative (RT-q) PCR. Total RNA was extracted from the cells ($1x10^6$ cells per well in a 6-well plate) using an EZ-press RNA Purification kit (cat. no. B0004DP; EZBioscience) and equal amounts of RNA were reverse-transcribed into cDNA using the First Strand cDNA Synthesis kit, ReverTraAce (cat. no. FSQ-201; Toyobo Life Science). RNA extraction and cDNA synthesis were performed according to the manufacturer's protocols. RT-qPCR was performed using a LightCycler 480 SYBR-Green I Master (Roche Diagnostics) according to the manufacturer's instructions. The thermocycling conditions were applied at 95˚C for 5 min, followed by 40 cycles of 95˚C for 10 sec (denaturation), 60˚C for 20 sec (annealing) and then at 72˚C for 20 sec (extension). mRNA expression was normalized to GAPDH using the $2^{-\Delta\Delta Cq}$ method (25). All the experiments were carried out at least three times independently. The primers used for RT-qPCR are listed in Table SI.

Western blot analysis. The cells were lysed by RIPA lysis buffer (cat. no. P0013K; Beyotime Institute of Biotechnology) containing a protease inhibitor cocktail (cat. no. 04693132001; Roche Diagnostics) on ice for 30 min. The protein concentration was determined using the BCA kit assay (cat. no. 23225; Thermo Fisher Scientific, Inc.). Total cellular proteins were extracted and analyzed by immunoblotting as described previously (23). In brief, a total of 30 μg of protein per lane were separated on 10% SDS-polyacrylamide gel and then transferred to PVDF membranes. Non-fat dried milk (5%; cat.no.1172GR500;BioFroxx) dissolved in TBST (Tris-buffered saline with 0.5% Tween-20, cat. no. 1115GR500; BioFroxx) was used to block at room temperature for 1 h. The corresponding primary antibodies were incubated overnight at 4˚C, followed by the addition of HRP-labeled secondary antibodies at room temperature for 1 h. Enhanced Chemiluminescence (ECL; cat. no. 34580; Thermo Fisher Scientific, Inc.) was employed for visualizing results Subsequently, images were acquired using a CCD system. Densitometry analysis was performed using ImageJ (Version v1.8.0; National Institutes of Health) software. The antibodies used for western blotting are listed in Table SII.

Chemoresistance assay. A CCK-8 assay was employed to evaluate the chemoresistance of non-OSCs and OSCs to doxorubicin (DOX) or cisplatin (CIS; cat. nos. HY-15142 and HY-17394; MedChemExpress). Cells were plated in 96-well

plates at a density of 5,000 cells/well. Different concentrations (0-25 μM) of CIS or (0-100 μM) DOX were added to the medium for 24 h. After treatments, 10% CCK-8 solution was added into mediums incubated for 2 h and optical density (OD) values were evaluated at 450 nm using a microplate reader. CIS and DOX were dissolved in dimethyl sulfoxide (DMSO) and the equivalent amount of DMSO was added to the control group for consistency in the present study.

Flow cytometry assay. The intracellular reactive oxygen species (ROS) were detected by the Reactive Oxygen Species Assay kit (cat. no. S0033S; Beyotime Institute of Biotechnology) which includes 2',7'-Dichlorodihydrofluorescein diacetate (DCFH-DA) detection. According to the kit protocol, cells were treated with 10 μM DCFH-DA diluted in DF12 for 20 min at 37˚C. Fluorescence was detected at 488 nm excitation and 525 nm emission using a Beckman MoFlo Astrios EQs flow cytometer (Beckman Coulter, Inc.). The flow cytometry data were analyzed using FlowJo v10 software (FlowJo LLC).

Analysis of NADPH and ATP. The intracellular NADPH levels were determined using an $NADP^+$/NADPH Assay kit with water-soluble tetrazolium salt 8 (cat. no. S0179; Beyotime Institute of Biotechnology). The absorbance values were measured at 450 nm by recording luminescence using a BioTek Synergy LX multimode reader (BioTek; Agilent Technologies, Inc.). The intracellular ATP levels were determined using an ATP assay kit (cat. no. S0026, Beyotime Institute of Biotechnology). Luminescence was recorded using the same multimode reader with an integration time of 10 sec per well. All the analyses were conducted according to the instructions of the manufacturer.

Fluorescent staining for mitochondria. Cells were seeded in glass-bottom dishes (Standard Imaging, Inc.) and treated with CIS or DOX. OSCs were initially cultured in normal petri dishes and then transferred to glass-bottom dishes for image capture. Cells were stained with PK Mito Red (PKMR) dye (cat. no. PKMR-2; GenVivo, Inc.) at 37˚C for 15 min. Images were acquired using a Multimodality Structured Illumination Microscopy (Multi-SIM) imaging system (NanoInsights-Tech) equipped with a 100, 1.49NA oil objective and a Kinetix camera (Photometrics). The PKMR was excited at a wavelength of 561 nm and the resulting images were acquired in 3D-SIM mode with a laser power of 50 mW and an exposure time of either 1 msec (for OSCs) or 2 msec (for non-OSCs). Subsequently, the acquired images were reconstructed using SIM Imaging Analyser software (Version 2.23.9, NanoInsights-Tech). During image acquisition, cells were maintained in a humidified chamber at 37˚C under 5% CO_2.

3D rendering. The acquired images were reconstructed using Imaris v9.6.0 (Oxford Instruments plc). The original images were observed in 3D view mode and the surface module was used for 3D rendering. The rendering parameter surface detail was 0.0612. The background subtraction mode was selected and the diameter of the largest sphere was 1 μm (for OSCs)/4 μm (for non-OSCs). The threshold and filter surfaces were adjusted according to the actual conditions of each image. After rendering, mitochondrial parameters including length, volume and sphericity of the mitochondrial network were obtained in a single cell for drawing the density distribution map.

Statistical analysis. The data were presented as the mean ± standard deviation. A one-way analysis of variance (ANOVA) followed by Tukey's multiple comparisons test was conducted to analyze the among multiple groups. An unpaired two-tailed Student's t-test was used to compare the data between two groups. $P<0.05$ was considered to indicate a statistically significant difference.

Results

OSCs exhibit distinct mitochondrial morphology compared with non-OSCs. To investigate the mitochondrial morphology of OSCs, OSCs were cultured in a serum-free culture medium as previously described (23,24). When cultured in DF12 supplemented with 5% FBS, cells exhibited characteristics of non-OSCs and demonstrated a monolayer phenotype (Fig. 1A). By contrast, under serum-free conditions, these cells exhibited characteristics of OSCs and displayed a sphere phenotype (Fig. 1A). To assess the chemoresistance of OSCs compared with non-OSCs, the cells were treated with primary clinical chemotherapeutics CIS and DOX. The results indicated that OSCs exhibited a higher level of chemoresistance to CIS or DOX treatment compared with non-OSCs (Fig. 1B). TUNEL staining was employed to assess the apoptotic status of the cells. Non-OSCs exhibited significant apoptosis upon treatment with CIS or DOX compared with the untreated group (Fig. 1C). However, only a few apoptotic cells were detected in the OSCs compared with the non-OSCs group (Fig. 1C). Compared with non-OSCs, OSCs showed significantly increased resistance to apoptosis (Fig. 1D). Overall, these results indicated that the OSCs showed higher chemoresistance compared with non-OSCs.

For an improved characterization and quantitative analysis of mitochondrial morphology and dynamic alteration, particularly fusion and fission status, high-quality mitochondrial images are essential. A schematic illustrated the process of capturing and rendering 3D images of cells (Fig. 2A). The complete structure and network of mitochondria within non-OSCs were visualized (Fig. 2B). This revealed a diverse range of morphologies in non-OSCs, including punctate shapes, linear forms and interconnected networks. Additionally, OSCs exhibited mitochondrial morphologies distinct from those observed in non-OSCs (Fig. 2C). For an improved characterization and quantitative analysis of mitochondrial morphology, videos were created to show the full range of mitochondrial morphologies in both individual non-OSCs and OSCs (Videos S1-S4). To further elucidate the differences in mitochondrial morphologies between non-OSCs and OSCs, the present study analyzed and quantified 10-20 cells for each group, measuring various morphological parameters of whole mitochondria, including length, volume and sphericity. Mitochondria in OSCs exhibited a predominant fusion pattern and reduced sphericity. These findings indicated that mitochondria within OSCs were characterized by increased size and enhanced fusion compared with non-OSCs.

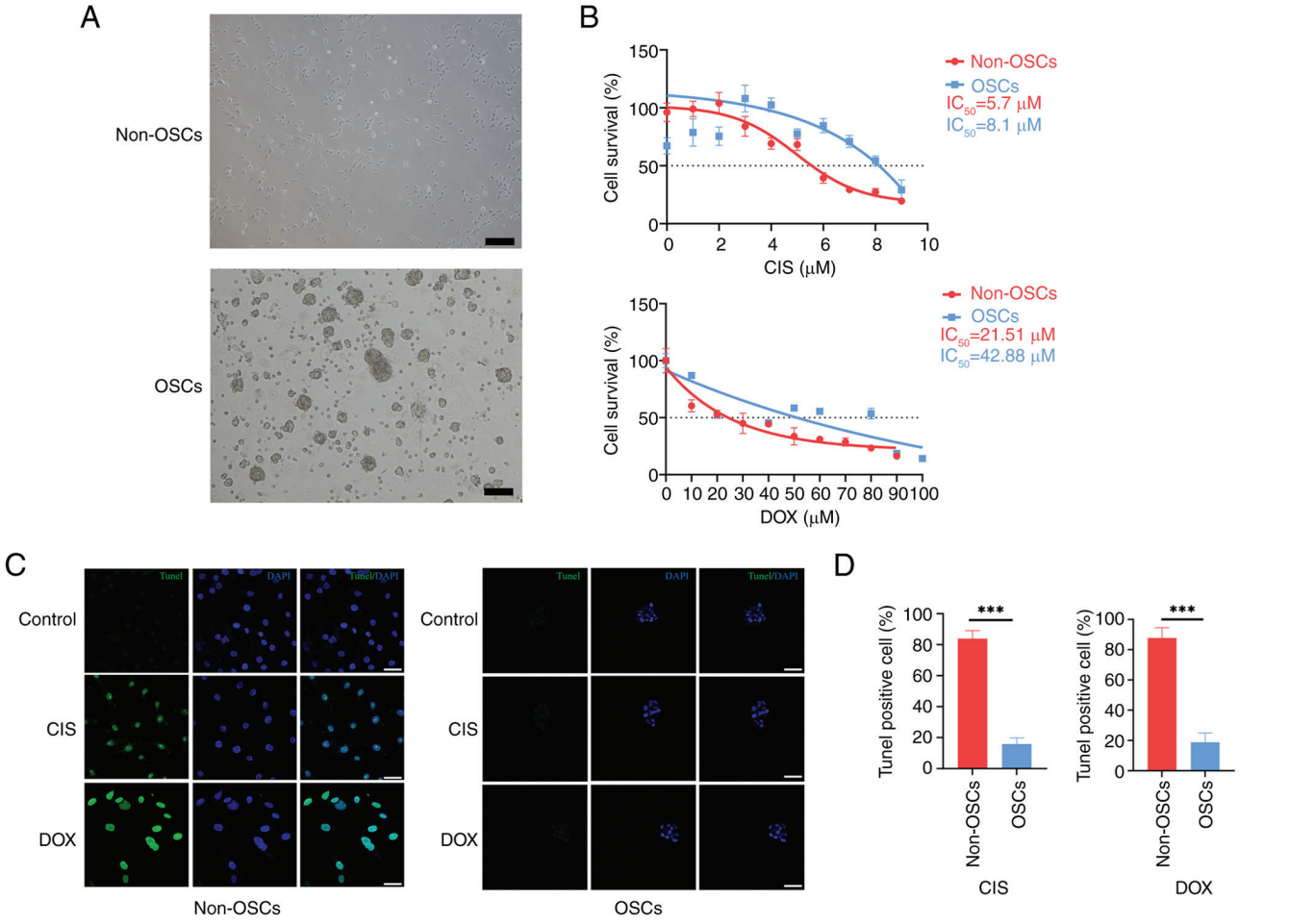

Figure 1. OSCs exhibit more resistance to chemotherapy than non-OSCs. (A) Morphology of non-OSCs and OSCs (scale bar, 200 μm). (B) Non-OSCs and OSCs cell survival curves and IC_{50} statistics treated with CIS and DOX. (C) TUNEL staining of apoptosis in non-OSCs and OSCs treated with CIS and DOX (green: TUNEL, blue: DAPI; scale bar, 50 μm). (D) Statistics of TUNEL positive cells (%). Data are presented as the mean ± SD of three independent experiments (n=3); ***P<0.001. OSCs, osteosarcoma stem cells; IC_{50}, half-maximal inhibitory concentration; CIS, cisplatin; DOX, doxorubicin.

OSCs exhibit stable mitochondrial homeostasis compared with non-OSCs upon chemotherapy. The diverse morphologies of mitochondria could influence mitochondrial functions, including cell survival, apoptosis, metabolism, ROS management and mitophagy (26,27). CIS or DOX triggers apoptosis through mitochondrial pathways involving the release of cytochrome *c*, generation of ROS and permeabilization mediated by Bax/Bak (28). Following treatment with CIS or DOX, non-OSCs showed higher levels of mitochondrial fragmentation and fission compared with the untreated group (Fig. 3A). Additionally, non-OSCs treated with CIS or DOX showed smaller mitochondrial volume and shorter length, with more homogeneous sphericity distribution compared with the untreated group (Fig. 3B and C). The mitochondrial networks of OSCs did not exhibit significant alterations and their overall morphology remained stable following CIS or DOX treatment (Fig. 3D). Moreover, CIS or DOX treatment did not affect the mitochondrial volume, length and sphericity distribution. These results suggested that CIS or DOX can induce mitochondrial fragmentation and fission in non-OSCs, while having no impact on OSCs. Mitochondria in OSCs exhibited more stable homeostasis compared with non-OSCs when exposed to chemotherapeutics.

OSCs show mitochondrial functional homeostasis, compared with non-OSCs, under chemotherapy. Disruption of mitochondrial homeostasis impairs mitochondrial function, affects cellular metabolism and can potentially lead to apoptosis (29). Mitochondria play a crucial role in regulating the metabolism and bioenergetics of cancer cells and their dysfunction can disrupt the production of essential metabolites such as ATP and NADPH (14). To assess mitochondrial function, specific assays were used to measure parameters related to ATP production, NADPH levels and ROS levels. Non-OSCs exhibited significantly reduced intracellular ATP levels following CIS or DOX treatment compared with the untreated group (Fig. 4A). The intracellular ATP levels in OSCs were unaffected by CIS or DOX treatment, compared with the untreated group (Fig. 4A). NADPH/NADP directly affects the redox balance within cells (30). Non-OSCs after the treatment with CIS or DOX showed a significant downregulation of the intracellular NADPH/($NADP^+$ + NADPH) ratio compared with the untreated group (Fig. 4B). However, there was no significant decrease in the NADPH/($NADP^+$ + NADPH) ratio observed in OSCs following CIS or DOX treatment (Fig. 4B). Intracellular ROS was detected by flow cytometry using DCFH-DA staining. The results demonstrated a significant increase in intracellular

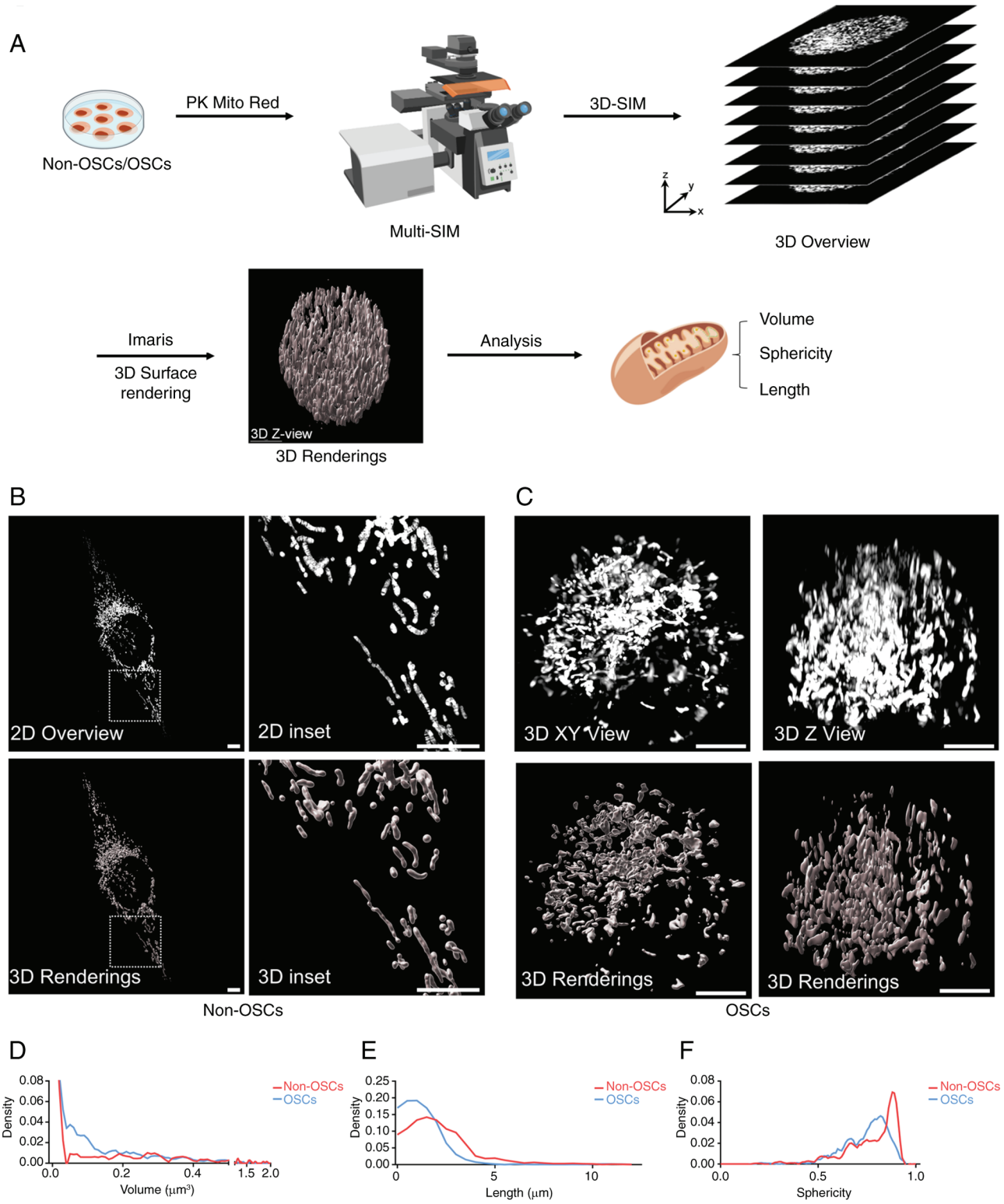

Figure 2. OSCs exhibit different mitochondrial morphologies compared with non-OSCs. (A) Schematic of the process used for capturing and rendering 3D images of cells. (B) Original mitochondrial images of non-OSCs obtained by Multi-SIM and their 3D reconstructions via software rendering, showing full view (right) and partial zoom-in (left). (C) Original mitochondrial images and 3D reconstructions of OSCs in XY view (right) and Z view (left). Density plot analyses of mitochondrial morphological parameters measuring (D) volume, (E) length and (F) sphericity (scale bar, 5 μm). OSCs, osteosarcoma stem cells; Multi-SIM, multimodality structured illumination microscopy.

ROS accumulation in non-OSCs following CIS and DOX treatment, whereas no substantial ROS accumulation was observed in OSCs following exposure to either CIS or DOX (Fig. 4D).

The regulation of mitochondrial dynamics involves specific proteins, including MFN1, MFN2, OPA1 and DRP1. The results of the present study showed that non-OSCs treated with CIS or DOX exhibited significant downregulation of

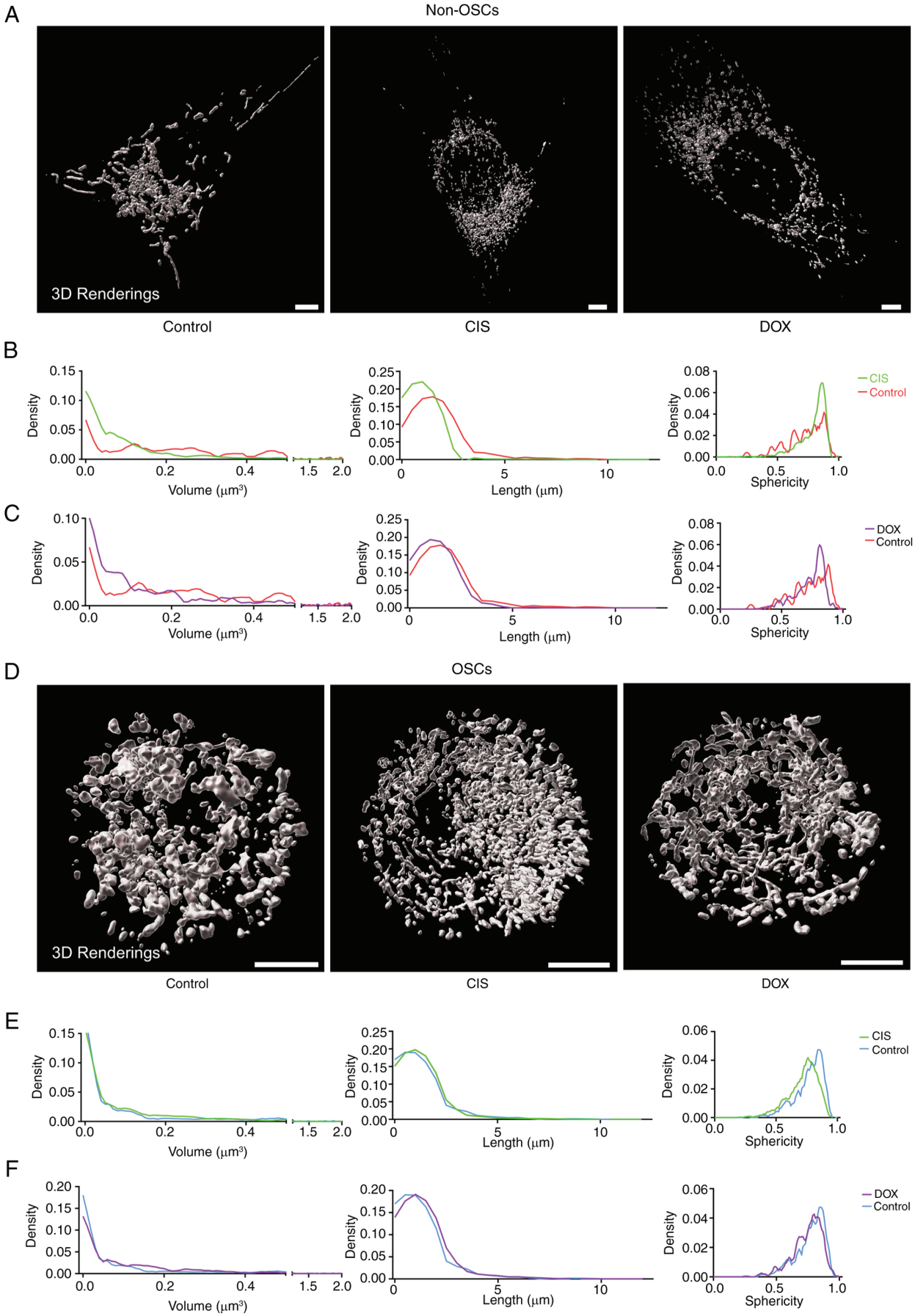

Figure 3. OSCs resist drug-induced mitochondrial fission. (A) 3D rendered mitochondrial images of non-OSCs treated with CIS and DOX (scale bar, 5 μm). (B and C) Density plot analyses measuring mitochondrial volume and length in non-OSCs treated with CIS (B) and DOX (C). (D) 3D rendered mitochondrial images of OSCs treated with CIS and DOX (scale bar, 5 μm) (E-F) Density plot analyses measuring mitochondrial volume and length in OSCs treated with (E) CIS and (F) DOX. OSCs, osteosarcoma stem cells; CIS, cisplatin; DOX, doxorubicin.

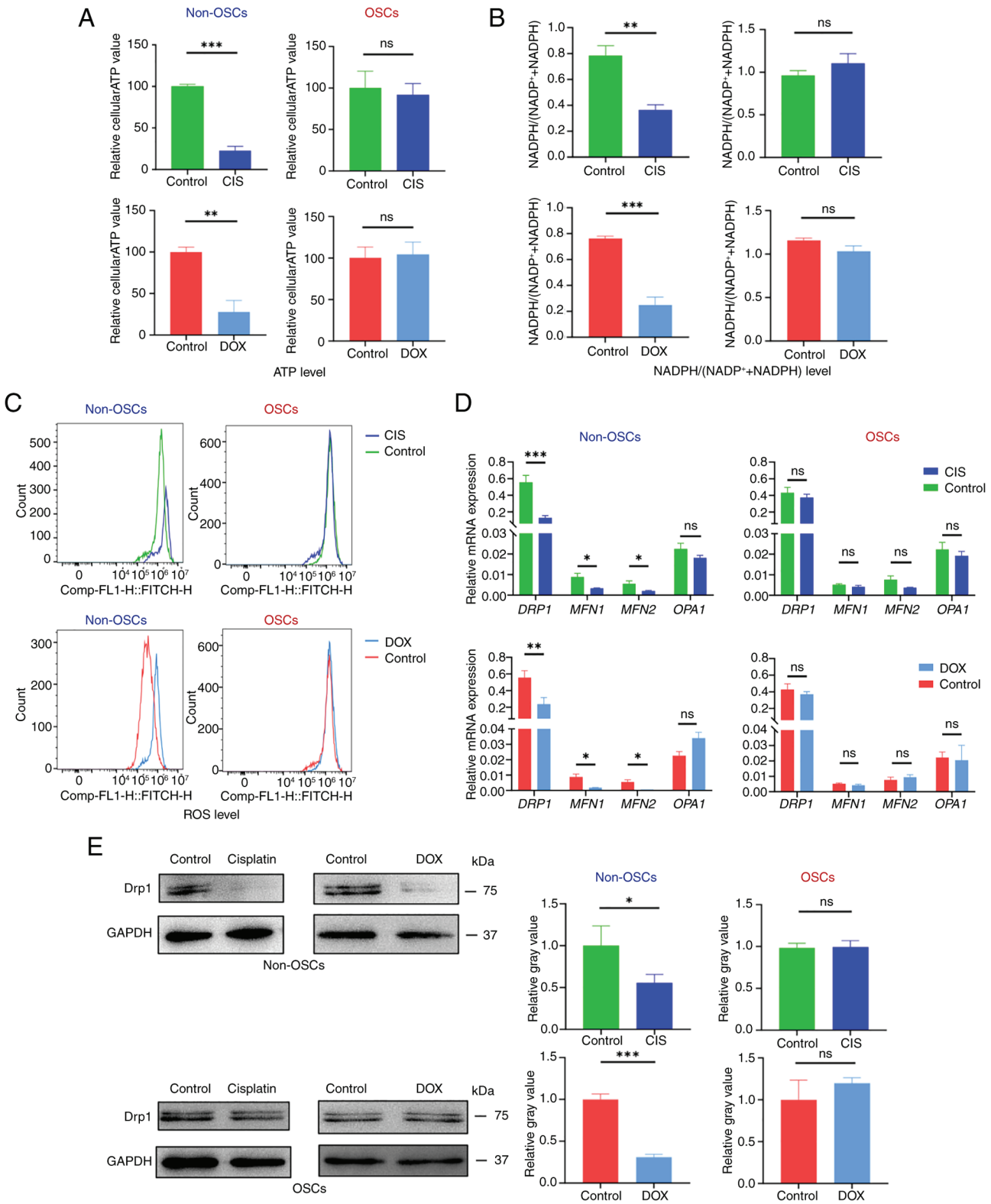

Figure 4. OSCs resist drug-induced mitochondrial functional damage. (A) Relative intracellular ATP generation per cell in non-OSCs and OSCs treated with CIS or DOX. (B) Relative intracellular NADPH/(NADP+NADPH) assay in non-OSCs and OSCs treated with CIS or DOX (C) ROS labeling with DCFH-DA in non-OSCs and OSCs treated with CIS or DOX. (D) Reverse transcription-quantitative PCR detecting the expression of mitochondrial fusion and fission-related genes (DRP1, MFN1, MFN2, OPA1) treated with CIS or DOX. (E) Western blot analysis showing DRP1 protein expression and relative gray value. Data are presented as the mean ± SD of three independent experiments (n=3); *P<0.05, **P<0.01, ***P<0.001, ns, not significance. OSCs, osteosarcoma stem cells; CIS, cisplatin; DOX, doxorubicin; ROS, reactive oxygen species; DCFH-DA, 2',7'-Dichlorodihydrofluorescein diacetate; DRP1, dynamin-related protein 1.

MFN1, MFN2 and DRP1 expression while showing no significant change in OPA1 expression. Conversely, in OSCs treated with CIS or DOX, the expression levels of MFN1, MFN2, DRP1 and OPA1 remained unchanged (Fig. 4D). Western

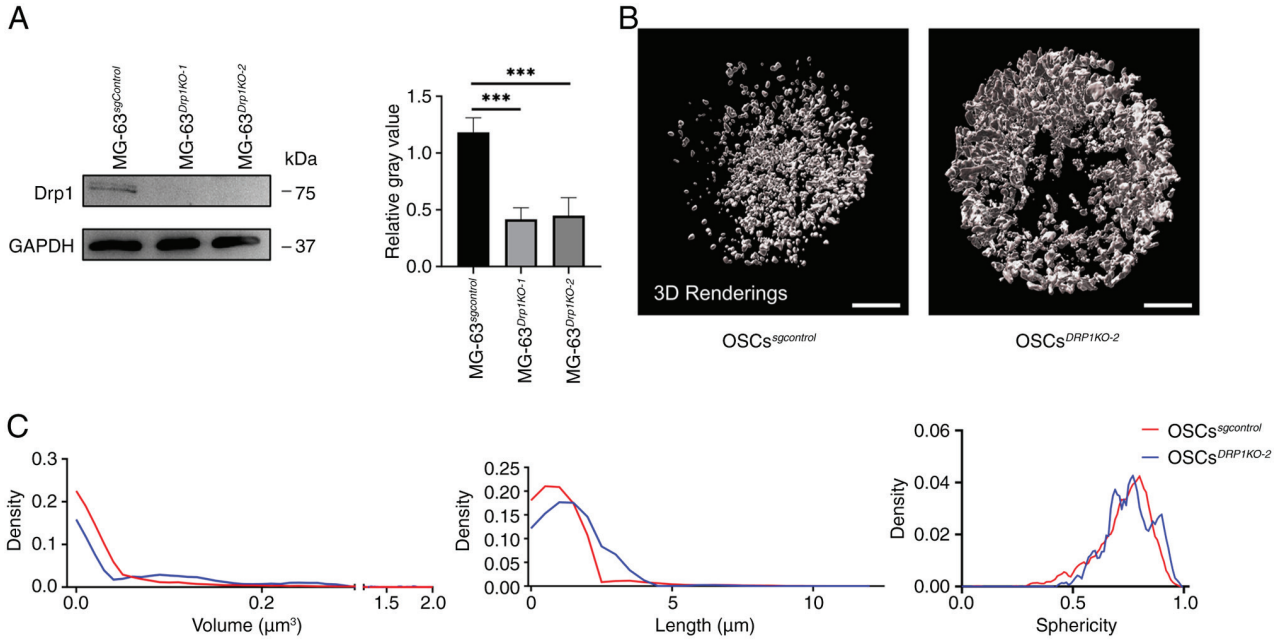

Figure 5. Knockdown of DRP1 induces mitochondrial morphological fission in OSCs. (A) CRISPR/Cas9 was used to knock out DRP1 expression and western blotting was used to determine knockout efficiency. (B) Original mitochondrial images and 3D rendered mitochondrial images of MG-63^{sgcontrol} and MG-63^{DRP1KO} (scale bar, 5 μm). (C) Density plot analysis measuring mitochondrial volume and length in non-OSCs and OSCs. Data are presented as the mean ± SD of three independent experiments (n=3); ***P<0.001. DRP1, dynamin-related protein 1; OSCs, osteosarcoma stem cells.

blot analysis was used to detect the protein expression level of DRP1, which showed that non-OSCs had significantly downregulated DRP1 expression following CIS and DOX treatment, while OSCs showed no significant change in DRP1 expression (Fig. 4E). The results suggested that CIS or DOX can induce mitochondrial dysfunction in non-OSCs but not in OSCs. Meanwhile, the expression of MFN1, MFN2 and fission-related DRP1 was downregulated following CIS or DOX treatment; however, this suppression of these genes in OSCs was not observed.

In summary, under CIS or DOX treatment, OSCs maintained mitochondrial stability without significant alterations in ATP or NADPH levels, ROS accumulation, or gene expression. Conversely, non-OSCs exhibited impaired mitochondrial function, characterized by reduced levels of ATP and NADPH, elevated ROS accumulation and suppressed gene expression. These results indicated that OSCs can maintain mitochondrial functional homeostasis during chemotherapy, whereas non-OSCs lack this ability.

DRP1 regulates mitochondrial morphology in OSCs. Changes in mitochondrial morphology are a continuous process, where mitochondria constantly undergo fusion and fission. Disruption of these processes can lead to dysregulated of mitochondrial homeostasis. The present study used two different sgRNA sequences to knock out DRP1 (OSCs$^{DRP1\text{-}KO}$, and OSCs$^{DRP1\text{-}KO2}$) and western blotting was employed to determine the knockout efficiency (Fig. 5A). The two sgRNA sequences demonstrated high knockdown efficiency and OSCs$^{DRP1\text{-}KO2}$ was selected for further experiments. After sequencing MG-63$^{DRP1\text{-}KO2}$, a 4-base pair deletion in exon 2 of the *DRP1* gene was identified, which caused a frameshift mutation that led to the production of a premature stop codon in exon 5, truncating the protein. This mutation affected the GTPase domain, which is crucial for GTP binding and hydrolysis, both of which are essential for the protein's role in mitochondrial and peroxisomal fission (Fig. S1). The mitochondrial morphology in OSCs$^{DRP1\text{-}KO2}$ showed increased fusion (Fig. 5B). Further quantitative analysis revealed an increase in mitochondrial volume and length in OSCs$^{DRP1\text{-}KO2}$ compared with the OSCs^{sgcontrol}. Additionally, the cellular sphericity distribution did not show any significant change (Fig. 5C). These findings indicate that DRP1 is essential for regulating mitochondrial fission and fusion processes and knockdown of DRP1 leads to significant alterations in the morphology of the mitochondrial network.

DRP1 affects OSC chemoresistance. To investigate the relationship between changes in mitochondrial morphology and chemoresistance, OSCs$^{DRP1\text{-}KO2}$ and OSCs^{sgcontrol} were treated with CIS or DOX at various concentrations. The results indicated that half-maximal inhibitory concentration (IC_{50}) was significantly decreased in OSCs$^{DRP1\text{-}KO2}$ following the treatments with CIS or DOX (Fig. 6A). TUNEL staining for apoptosis revealed a significant increase in fluorescence in the OSCs$^{DRP1\text{-}KO2}$ compared with the OSCs^{sgcontrol} treated with CIS or DOX (Fig. 6B). Furthermore, parameters representing mitochondrial function were assessed. OSCs$^{DRP1\text{-}KO2}$ exhibited a significant decrease in average intracellular ATP production (Fig. 6C) following CIS or DOX treatment compared with the untreated group. Intracellular NADPH/($NADP^+$+NADPH) in OSCs$^{Drp\text{-}1KO2}$ showed a significant downregulation following CIS or DOX treatment compared with the untreated group (Fig. 6D). Additionally, knocking out DRP1 in OSCs led to significant intracellular ROS accumulation and reduced chemoresistance following CIS and DOX treatment compared with OSCs^{sgcontrol} (Fig. 6E). These results underscore the critical role of DRP1 in maintaining chemoresistance and mitochondrial function in OSCs.

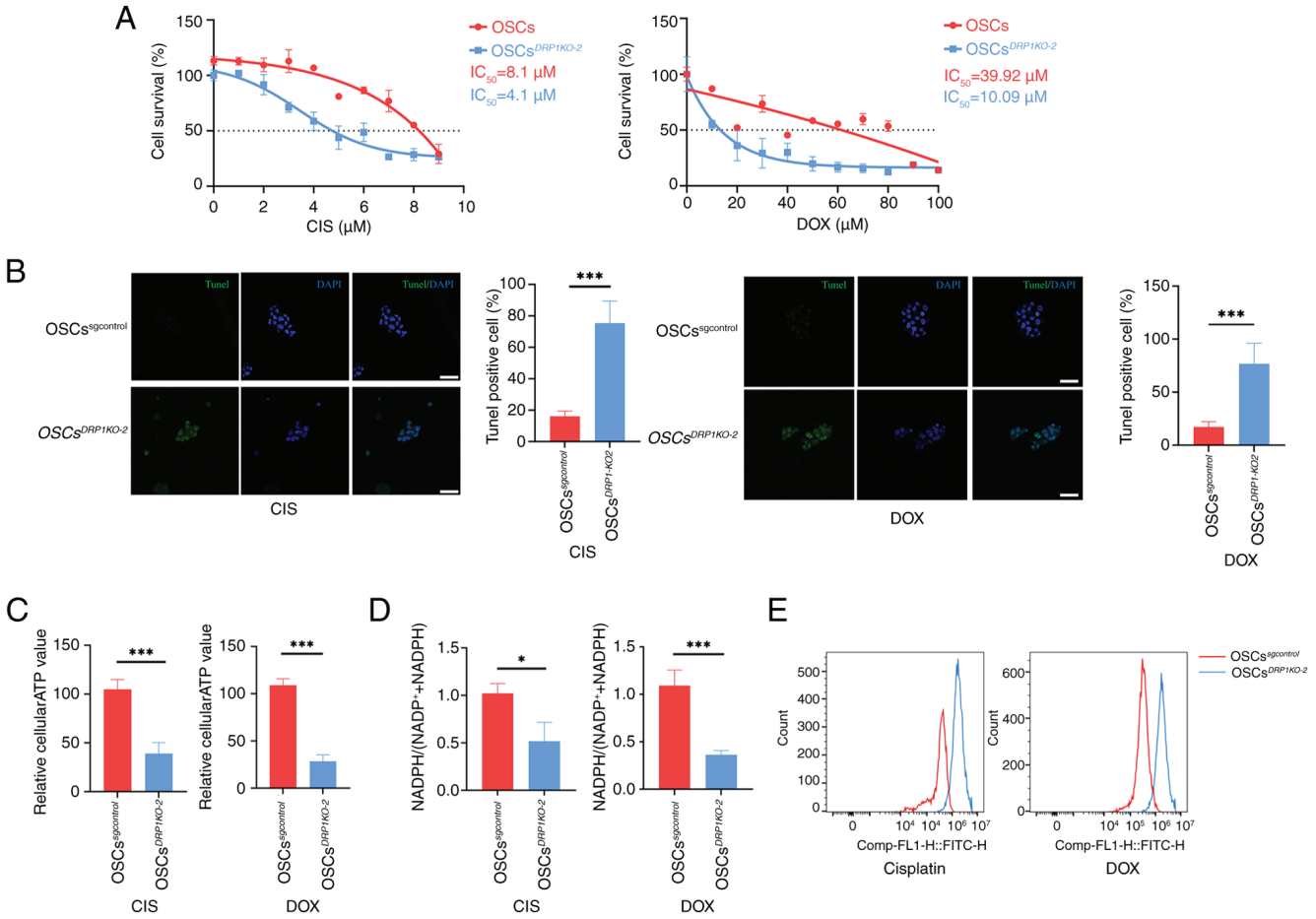

Figure 6. DRP1 affects OSCs chemoresistance. (A) Survival curves and IC_{50} statistics for OSCs and $OSCs^{DRP1KO-2}$ cells treated with CIS and DOX. (B) TUNEL staining of apoptosis in OSCs and $OSCs^{DRP1KO-2}$ treated with CIS and DOX and statistics of TUNEL positive cells; green: TUNEL, blue: DAPI, scale bar, 50 μm). (C) Relative intracellular ATP generation per cell in OSCs and $OSCs^{DRP1KO-2}$ treated with CIS or DOX. (D) Relative intracellular NADPH/($NADP^+$+NADPH) assay in OSCs and $OSCs^{DRP1KO-2}$ treated with CIS or DOX. (E) ROS labeling with DCFH-DA in OSCs and $OSCs^{DRP1KO-2}$ treated with CIS or DOX. Data are presented as the mean ± SD of three independent experiments (n=3); *P<0.05, ***P<0.001. DRP1, dynamin-related protein 1; OSCs, osteosarcoma stem cells; IC_{50}, half-maximal inhibitory concentration; CIS, cisplatin; DOX, doxorubicin; ROS, reactive oxygen species.

Discussion

Chemoresistance in cancer cells is a major cause of poor prognosis in patients. Our previous studies have shown that non-OSCs can be reprogrammed into OSCs, which subsequently acquire higher chemoresistance (23,24,31). However, the mechanisms underlying this increased chemoresistance in OSCs remain unclear. The present study discovered a potential mechanism of chemoresistance in osteosarcoma cells. OSCs counteract apoptosis and mitochondrial dysfunction induced by chemotherapy by maintaining mitochondrial homeostasis through the fission gene DRP1, suggesting a potential target for eliminating OSCs.

Cancer stem cells (CSCs) demonstrate significantly enhanced chemoresistance compared with non-CSCs, attributed to multiple complex mechanisms (32). Elevated expression of ATP-binding cassette (ABC) transporters (33) and augmented DNA damage repair capabilities were notable (34). Additionally, enhanced chemoresistance is attributed to alterations in the expression levels of anti-apoptotic proteins, such as Bcl-2 and BAX (35), along with the reprogramming of metabolic pathways (36). As well as these mechanisms, the present study investigated the mechanisms of chemoresistance in OSCs from the perspective of mitochondrial stability. OSCs exhibited more stable mitochondrial homeostasis compared with non-OSCs, both in terms of morphology and function. Cancer cells with enlarged and fused mitochondria typically demonstrate heightened chemoresistance through the maintenance of elevated ATP levels and the mitigation of oxidative stress (37). The present study demonstrated that OSCs were able to maintain stable ATP and NADPH production under CIS or DOX-induced stress, whereas non-OSCs could not. Vlashi *et al* (38) similarly demonstrated metabolic differences between CSCs and non-CSCs in glioma; CSCs were able to maintain higher ATP levels under stress and exhibited enhanced mitochondrial repair capabilities. The accumulation of ROS could induce apoptosis by causing a decrease in mitochondrial membrane potential, leading to the release of cytochrome *c* from the mitochondria into the cytosol, which then triggered a cascade of apoptotic events. Another study found that breast cancer CSCs could resist radiotherapy by clearing ROS through the synthesis of glutathione genes, thereby inhibiting apoptosis (39). The present study found that OSCs were able to resist chemotherapeutics by preventing the accumulation of ROS by maintaining mitochondrial homeostasis, which further elucidated the mechanism behind the difficulty of targeting CSCs for elimination in clinical settings.

Regarding mitochondrial morphology, there are few widely recognized conclusions about the differences between CSCs and non-CSCs and the results from various studies remained controversial. Civenni *et al* (40) indicated that BRD4 promotes mitochondrial fission and sustains the survival of CSCs by regulating the expression of the mitochondrial fission factor. Inhibiting BRD4 impedes mitochondrial fission, leading to mitochondrial dysfunction and the senescence and exhaustion of CSCs. The same conclusions were validated in brain tumor-initiating cells (BTICs), where BTICs exhibited a more fragmented mitochondrial morphology compared with non-BTICs, indicating increased mitochondrial fission within BTICs. DRP1, a key mediator protein of mitochondrial fission, was activated in BTICs but inhibited in non-BTICs (41). However, mitochondrial dynamics in breast cancer involve different mechanisms. Wu *et al* (42) indicate that epithelial-mesenchymal transition (EMT) promotes mitochondrial fusion by upregulating the expression of MFN1, enhancing antioxidant capacity and thus sustaining the self-renewal and expansion of CSCs. The study demonstrated that mitochondrial dynamics in breast CSCs tend towards fusion. Research in esophageal squamous cell carcinoma demonstrated that CSCs induced mitochondrial fission through the activation of the key autophagy protein Parkin, which is activated by EMT and leads to mitophagy (43). The aforementioned results indicate that mitochondrial morphology is complex in CSCs across different tissues and can be regulated by a variety of mechanisms. The findings of the present study revealed significant disparities in mitochondrial morphology between non-OSCs and OSCs. Notably, the mitochondria in OSCs exhibited a higher degree of fusion, resulting in a more interconnected mitochondrial network compared with non-OSCs. Notably, the mitochondrial network with more interconnection showed more stable homeostasis under the stress of chemotherapy CIS and DOX. This increased mitochondrial fusion helped reduce chemosensitivity in OSCs, thereby promoting chemoresistance. Moreover, the regulation of this mitochondrial network was facilitated by the expression of the mitochondrial fission protein DRP1. The present study revealed the critical role of DRP1 in OSCs, particularly in maintaining their chemoresistance through the regulation of mitochondrial dynamics. The high expression of DRP1 is crucial for sustaining the proliferation and survival of OSCs, making it a potential therapeutic target. These findings provide a significant basis for the future development of cancer treatment strategies targeting DRP1.

CIS and DOX can both induce DNA damage. CIS forms DNA cross-links, inhibiting DNA replication and transcription, while DOX intercalates into DNA, disrupting the function of topoisomerase II and leading to DNA strand breaks (44). In the present study, OSCs exhibited no differences in resistance to these two chemicals, suggesting that mitochondrial dynamics may involve a similar mechanism and resistance effect in countering chemotherapeutics that induce apoptosis through DNA damage. The results supplemented the finding on mitochondrial dynamics between OSCs and non-OSCs, offering a new direction for further research into the chemoresistance of OSCs. In fact, the role of MFN1 in the chemoresistance of OSCs was also detected. However, MFN1 was expressed at a very low level in osteosarcoma (data not shown).

Live-cell 3D imaging presented challenges due to various limitations, including probe photobleaching, rapid mitochondrial mobility and, most critically, phototoxicity, especially for suspension cells. Phototoxic effects accumulate from repeated scanning during Z-stacking, leading to continuous swelling artifacts. Moreover, the results displayed the 3D mitochondrial structure of OSCs, suspension cells, without any occurrence of phototoxicity or continuous swelling artifacts. Another classical approach to studying mitochondrial dynamics involves the use of electron microscopy, which, although offering high resolution, can only observe fixed cells and cannot replicate the mitochondrial state in living cells. By contrast, the method of the present study allowed for the observation of mitochondria in living cells and enabled continuous imaging to monitor dynamic changes in the mitochondrial network. The present study provided a new experimental approach for exploring changes in mitochondrial dynamics within live cells.

In conclusion, the present study showed a novel mechanism of chemoresistance in OSCs from a mitochondrial dynamics perspective. This provided new insights into chemoresistance in CSCs and suggested potential therapeutic targets for the elimination of OSCs in clinical settings.

Acknowledgements

The authors appreciate the support of Ms. Jialing Xu (Core Facilities of Life Sciences, School of Life Sciences, Sun Yat-sen University, Guangdong, China) for equipment support and technical assistance.

Funding

The present study was supported by a grant from the Programs of Guangdong Science and Technology (grant no. 2019B1515210015), China Postdoctoral Science Foundation (grant no. 2023M744083) and National Natural Science Foundation of China (grant no. 31871413).

Availability of data and materials

The datasets used and/or analyzed during the current study are available from the corresponding author on reasonable request.

Authors' contributions

BT performed the experiments, analyzed the data, conceived the study, wrote the original draft, reviewed and edited the manuscript. YW performed the experiments, analyzed the data, wrote the original draft, reviewed and edited the manuscript. XD performed the experiments. YZ wrote, reviewed and edited the manuscript, supervised and administered the project and was responsible for funding acquisition.

Ethics approval and consent to participate

Not applicable.

Patient consent for publication

Not applicable.

Competing interests

The authors declare that they have no conflicts of interest.

References

1. Friedman JR and Nunnari J: Mitochondrial form and function. Nature 505: 335-343, 2014.
2. Labbé K, Murley A and Nunnari J: Determinants and functions of mitochondrial behavior. Annu Rev Cell Dev Biol 30: 357-391, 2014.
3. Xing J, Qi L, Liu X, Shi G, Sun X and Yang Y: Roles of mitochondrial fusion and fission in breast cancer progression: A systematic review. World J Surg Oncol 20: 331, 2022.
4. Giacomello M, Pyakurel A, Glytsou C and Scorrano L: The cell biology of mitochondrial membrane dynamics. Nat Rev Mol Cell Biol 21: 204-224, 2020.
5. Wai T and Langer T: Mitochondrial dynamics and metabolic regulation. Trends Endocrinol Metab 27: 105-117, 2016.
6. Eisner V, Picard M and Hajnóczky G: Mitochondrial dynamics in adaptive and maladaptive cellular stress responses. Nat Cell Biol 20: 755-765, 2018.
7. Vyas S, Zaganjor E and Haigis MC: Mitochondria and Cancer. Cell 166: 555-566, 2016.
8. Boulton DP and Caino MC: Mitochondrial fission and fusion in tumor progression to metastasis. Front Cell Dev Biol 10: 849962, 2022.
9. Quintana-Cabrera R and Scorrano L: Determinants and outcomes of mitochondrial dynamics. Mol Cell 83: 857-876, 2023.
10. Chan DC: Mitochondrial dynamics and its involvement in disease. Annu Rev Pathol 15: 235-259, 2020.
11. Rodrigues T and Ferraz LS: Therapeutic potential of targeting mitochondrial dynamics in cancer. Biochem Pharmacol 182: 114282, 2020.
12. Zacharioudakis E and Gavathiotis E: Mitochondrial dynamics proteins as emerging drug targets. Trends Pharmacol Sci 44: 112-127, 2023.
13. Kumar S, Ashraf R and C KA: Mitochondrial dynamics regulators: Implications for therapeutic intervention in cancer. Cell Biol Toxicol 38: 377-406, 2022.
14. Zeng X, Zhang YD, Ma RY, Chen YJ, Xiang XM, Hou DY, Li XH, Huang H, Li T and Duan CY: Activated Drp1 regulates p62-mediated autophagic flux and aggravates inflammation in cerebral ischemia-reperfusion via the ROS-RIP1/RIP3-exosome axis. Mil Med Res 9: 25, 2022.
15. Chuang KC, Chang CR, Chang SH, Huang SW, Chuang SM, Li ZY, Wang ST, Kao JK, Chen YJ and Shieh JJ: Imiquimod-induced ROS production disrupts the balance of mitochondrial dynamics and increases mitophagy in skin cancer cells. J Dermatol Sci 98: 152-162, 2020.
16. Jiang Y, Krantz S, Qin X, Li S, Gunasekara H, Kim YM, Zimnicka A, Bae M, Ma K, Toth PT, *et al*: Caveolin-1 controls mitochondrial damage and ROS production by regulating fission-fusion dynamics and mitophagy. Redox Biol 52: 102304, 2022.
17. Wu Z, Xiao C, Long J, Huang W, You F and Li X: Mitochondrial dynamics and colorectal cancer biology: Mechanisms and potential targets. Cell Commun Signal 22: 91, 2024.
18. Harrington JS, Ryter SW, Plataki M, Price DR and Choi AMK: Mitochondria in health, disease and aging. Physiol Rev 103: 2349-2422, 2023.
19. Zhang Y, Mai Q, Zhang X, Xie C and Zhang Y: Microenvironment signals and mechanisms in the regulation of osteosarcoma. In: Osteosarcoma-Biology, Behavior and Mechanisms. Honoki K and Weiss KR (eds). InTech, 2017.
20. Tian B, Du X, Zheng S and Zhang Y: The role of tumor microenvironment in regulating the plasticity of osteosarcoma cells. Int J Mol Sci 23: 16155, 2022.
21. Arima Y, Nobusue H and Saya H: Targeting of cancer stem cells by differentiation therapy. Cancer Sci 111: 2689-2695, 2020.
22. Batlle E and Clevers H: Cancer stem cells revisited. Nat Med 23: 1124-1134, 2017.
23. Zhang Y, Pan Y, Xie C and Zhang Y: miR-34a exerts as a key regulator in the dedifferentiation of osteosarcoma via PAI-1-Sox2 axis. Cell Death Dis 9: 777, 2018.
24. Pan Y, Zhang Y, Tang W and Zhang Y: Interstitial serum albumin empowers osteosarcoma cells with FAIM2 transcription to obtain viability via dedifferentiation. In Vitro Cell Dev Biol Anim 56: 129-144, 2020.
25. Livak KJ and Schmittgen TD: Analysis of relative gene expression data using real-time quantitative PCR and the 2(-Delta Delta C(T)) Method. Methods 25: 402-408, 2001.
26. Youle RJ and Karbowski M: Mitochondrial fission in apoptosis. Nat Rev Mol Cell Biol 6: 657-663, 2005.
27. Sheridan C and Martin SJ: Mitochondrial fission/fusion dynamics and apoptosis. Mitochondrion 10: 640-648, 2010.
28. Fulda S: Regulation of apoptosis pathways in cancer stem cells. Cancer Lett 338: 168-173, 2013.
29. Vasileiou PVS, Evangelou K, Vlasis K, Fildisis G, Panayiotidis MI, Chronopoulos E, Passias PG, Kouloukoussa M, Gorgoulis VG and Havaki S: Mitochondrial homeostasis and cellular senescence. Cells 8: 686, 2019.
30. Lin W, Lu X, Yang H, Huang L, Huang W, Tang Y, Liu S, Wang H and Zhang Y: Metabolic heterogeneity protects metastatic mucosal melanomas cells from ferroptosis. Int J Mol Med 50: 124, 2022.
31. Zhang H, Wu H, Zheng J, Yu P, Xu L, Jiang P, Gao J, Wang H and Zhang Y: Transforming growth factor β1 signal is crucial for dedifferentiation of cancer cells to cancer stem cells in osteosarcoma. Stem Cells 31: 433-446, 2013.
32. Chu X, Tian W, Ning J, Xiao G, Zhou Y, Wang Z, Zhai Z, Tanzhu G, Yang J and Zhou R: Cancer stem cells: Advances in knowledge and implications for cancer therapy. Signal Transduct Target Ther 9: 170, 2024.
33. Li Y, Wang Z, Ajani JA and Song S: Drug resistance and Cancer stem cells. Cell Commun Signal 19: 19, 2021.
34. Garcia-Mayea Y, Mir C, Masson F, Paciucci R and LLeonart ME: Insights into new mechanisms and models of cancer stem cell multidrug resistance. Semin Cancer Biol 60: 166-180, 2020.
35. Zheng Q, Zhang M, Zhou F, Zhang L and Meng X: The breast cancer stem cells traits and drug resistance. Front Pharmacol 11: 599965, 2021.
36. De Angelis ML, Francescangeli F, La Torre F and Zeuner A: Stem cell plasticity and dormancy in the development of cancer therapy resistance. Front Oncol 9: 626, 2019.
37. Genovese I, Carinci M, Modesti L, Aguiari G, Pinton P and Giorgi C: Mitochondria: Insights into crucial features to overcome cancer chemoresistance. Int J Mol Sci 22: 4770, 2021.
38. Vlashi E, Lagadec C, Vergnes L, Matsutani T, Masui K, Poulou M, Popescu R, Della Donna L, Evers P, Dekmezian C, *et al*: Metabolic state of glioma stem cells and nontumorigenic cells. Proc Natl Acad Sci USA 108: 16062-16067, 2011.
39. Diehn M, Cho RW, Lobo NA, Kalisky T, Dorie MJ, Kulp AN, Qian D, Lam JS, Ailles LE, Wong M, *et al*: Association of reactive oxygen species levels and radioresistance in cancer stem cells. Nature 458: 780-783, 2009.
40. Civenni G, Bosotti R, Timpanaro A, Vàzquez R, Merulla J, Pandit S, Rossi S, Albino D, Allegrini S, Mitra A, *et al*: Epigenetic control of mitochondrial fission enables self-renewal of stem-like tumor cells in human prostate cancer. Cell Metab 30: 303-318. e6, 2019.
41. Xie Q, Wu Q, Horbinski CM, Flavahan WA, Yang K, Zhou W, Dombrowski SM, Huang Z, Fang X, Shi Y, *et al*: Mitochondrial control by DRP1 in brain tumor initiating cells. Nat Neurosci 18: 501-510, 2015.
42. Wu MJ, Chen YS, Kim MR, Chang CC, Gampala S, Zhang Y, Wang Y, Chang CY, Yang JY and Chang CJ: Epithelial-Mesenchymal transition directs stem cell polarity via regulation of mitofusin. Cell Metab 29: 993-1002 e6, 2019.
43. Whelan KA, Chandramouleeswaran PM, Tanaka K, Natsuizaka M, Guha M, Srinivasan S, Darling DS, Kita Y, Natsugoe S, Winkler JD, *et al*: Autophagy supports generation of cells with high CD44 expression via modulation of oxidative stress and Parkin-mediated mitochondrial clearance. Oncogene 36: 4843-4858, 2017.
44. Duyndam MC, van Berkel MP, Dorsman JC, Rockx DA, Pinedo HM and Boven E: Cisplatin and doxorubicin repress Vascular Endothelial Growth Factor expression and differentially down-regulate Hypoxia-inducible Factor I activity in human ovarian cancer cells. Biochem Pharmacol 74: 191-201, 2007.